



Size-dependent MR relaxivities of magnetic nanoparticles

Alexander Joos^{a,*}, Norbert Löwa^b, Frank Wiekhorst^b, Bernhard Gleich^a, Axel Haase^a

^a Zentralinstitut für Medizintechnik (IMETUM), Technische Universität München, Boltzmannstraße 11, 85748 Garching, Germany

^b Physikalisch-Technische Bundesanstalt, Abbestraße 2-12, 10587 Berlin, Germany



ARTICLE INFO

Keywords:

Magnetic nanoparticles
Quantitative imaging
MR relaxometry
Hydrodynamic fractionation
Magnetic particle spectroscopy

ABSTRACT

Magnetic nanoparticles (MNPs) can be used as carriers for magnetic drug targeting and for stem cell tracking by magnetic resonance imaging (MRI). For these applications, it is crucial to quantitatively determine the spatial distribution of the MNP concentration, which can be approached by MRI relaxometry. Theoretical considerations and experiments have shown that R_2 relaxation rates are sensitive to the aggregation state of the particles, whereas R_2^* is independent of aggregation state and therefore suited for MNP quantification if the condition of static dephasing is met. We present a new experimental approach to characterize an MNP system with respect to quantitative MRI based on hydrodynamic fractionation. The first results qualitatively confirm the outer sphere relaxation theory for small MNPs and show that the two commercial MRI contrast agents Resovist[®] and Endorem[®] should not be used for quantitative MRI because they do not fulfill the condition for static dephasing. Our approach could facilitate the choice of MNPs for quantitative MRI and help clarifying the relationship between size, magnetism and relaxivity of MNPs in the future.

1. Introduction

Various types of nanoparticles are used in biomedical applications. Magnetic nanoparticles (MNPs) are especially promising because of their multi-functional capabilities such as bioseparation, transfections, hyperthermia, targeted delivery of drugs and stem cell tracking [1–3]. For the latter two it is crucial to quantitatively determine the spatial distribution of the concentration and the aggregation state of the MNPs to monitor and improve the efficacy of the application. Quantitative imaging of MNPs is enabled by magnetic resonance (MRI) and magnetic particle imaging (MPI). While MNP specific MPI is inherently quantitative, MRI detects magnetic particles non-specifically by measuring the effect of local field disturbance.

Theoretical considerations, simulations and experiments have shown that the MR relaxation rates R_2 and R_2^* strongly depend on the size of the MNPs or aggregates, respectively [4–9]. Three different regimes can be distinguished, with aggregates being treated the same way as particles using adapted overall hydrodynamic diameters d_{Hyd} and saturation magnetizations M_S . For small particles and aggregates that satisfy the motional averaging condition $\Delta\omega\tau_D < 1$ the quantum mechanical outer sphere theory applies. This theory predicts a quadratic dependence of the relaxation rates with the MNP size [4]:

$$R_2 = R_2^* = \frac{16}{45} f (\Delta\omega)^2 \tau_D \propto d_{\text{Hyd}}^2 \quad (1)$$

where $\Delta\omega = \gamma \frac{\mu_0}{3} M_S$ is the angular frequency shift at the particle surface compared with a point infinitely far away, γ is the gyromagnetic ratio of the proton, μ_0 the vacuum permeability, $\tau_D = \frac{d_{\text{Hyd}}^2}{D}$ the diffusion correlation time, D the self diffusion coefficient of water and f the volume fraction of the particles in the sample, which can be converted into the iron concentration. R_2 and R_2^* are equal only if the inhomogeneity of the B_0 field of the MR magnet can be neglected. Motional averaging means that the dephasing of the water protons due to the presence of the MNPs is averaged out by diffusion. With increasing particle size, this mechanism becomes less efficient resulting in an increase of relaxation rates. For particles that are too big to satisfy the motional averaging condition ($\Delta\omega\tau_D > 1$), the relaxation behaviour can be described by the static dephasing regime (SDR) model [10]:

$$R_2 = R_2^* = \frac{2\pi}{3\sqrt{3}} f \Delta\omega \quad (2)$$

Here, the relaxation rates only depend on the volume fraction and not on the particle size. Static dephasing refers to the dephasing of motionless water protons in the field created by the MNPs. For even larger particles, refocusing pulses become efficient and R_2 decreases again according to the partial refocusing model [4], while R_2^* remains the same:

$$R_2 = 2.25 \frac{x^{1/3}}{\tau_D} [1.34 + fx]^{5/3} < R_2^* \quad (3)$$

* Corresponding author.

E-mail address: ajoons@tum.de (A. Joos).

where $x = \sqrt{4/5} \gamma \frac{\mu_0}{3} M_S \tau_{CP}$ and τ_{CP} is the echo time.

This size-dependent behaviour shows that R_2 measurements can be used to assess the aggregation state of the MNPs whereas R_2^* measurements are independent of aggregation state and therefore suited for MNP quantification if the condition of static dephasing is met [11]. To allow a reliable quantification by MRI relaxometry, it is therefore essential to test whether the used particles are big enough to satisfy the SDR condition. In practice however, this is complicated by the size distribution of the particles.

We present here a new experimental approach to characterize an MNP system with respect to quantitative MRI. Our method is based on hydrodynamic fractionation producing MNPs with different well-defined sizes and subsequent geometric, magnetic and MR relaxation characterization of the fractions. This enables us to test the suitability of the MNP system for quantitative MRI and verify the theoretical predictions for the size dependence of relaxation rates at the same time. We applied our approach to the two commercially available MNP systems Resovist® and Endorem®.

2. Material and methods

2.1. Material

We used Ferucarbotran supplied by Meito Sangyo (JPN), which is a precursor of the commercial MRI contrast agent Resovist®, and Endorem® (namely ferumoxide) purchased from Guerbet (FRA). Both are aqueous suspensions of iron oxide nanoparticles and are approved specifically as MRI liver contrast agents. Whereas Resovist® is known to contain single and multi-core MNPs coated with dextran [12,13], Endorem consists only of multi-core MNPs coated by a thin dextran layer [14,15]. Transmission electron microscopy images can be found in [16,17] for Resovist® and in [14,15] for Endorem®.

Deionized water containing 0.2% (v/v) FL70 detergent (Fisher Sci., USA) was used as carrier liquid for hydrodynamic fractionation.

2.2. Hydrodynamic fractionation

The fractionation was performed using an asymmetric flow field-flow system (abbr. A4F; AF2000, Postnova Analytics GmbH, Germany) as described in [13] and fractions were collected from 5 (Resovist®) and 3 (Endorem®) consecutive runs. A4F is based on an elution method where the hydrodynamic diameter d_{Hyd} of an MNP is related to its retention time within a separation channel. The channel outlet was directly coupled to the UV detector, followed by MALS, DLS and finally MPS.

2.3. Size characterization by DLS and MALS

Hydrodynamic diameters were determined by dynamic light scattering (DLS) using a Malvern Instruments particle sizer (Zetasizer Nano ZS, Malvern Instruments, UK; $\lambda=633$ nm). In addition, we used multi-angle laser light scattering (abbr. MALS; PN3621, Postnova Analytics GmbH; $\lambda=532$ nm) to measure the angular dependence of scattered light on MNP size fractions. From this we derived the radius of gyration r_G using the intensity distribution function for spherical particles. The core diameter d_C was calculated by the following equation: $d_C = \sqrt{20/3} * r_G$. As small MNPs scatter light isotropically, the lowest detectable d_C is about 20 nm [18].

2.4. Magnetic characterization by MPS

The samples were magnetically characterized by Magnetic Particle Spectroscopy (MPS) using a commercial MPS device (MPS-3, Bruker BioSpin, Germany). Based on the same physical principle as MPI, waiving of any spatial encoding, MPS detects the non-linear dynamic magnetic susceptibility of MNPs. MPS is proven to be a straightforward

technique for specific quantification and characterization of MNPs [19], and allows for validation and improved understanding of MR relaxation measurement results. During an MPS measurement, a sinusoidal excitation is applied to the sample. Due to the non-linear magnetization curve of the MNPs, the measured magnetic response contains odd multiples of the excitation frequency, which can be visualized by a Fourier transform. Therefore, the MPS signal depends on the effective magnetic moment of the MNPs.

Here, the spectral magnetic moment of the third harmonic divided by the iron content is used.

2.5. Relaxation rate measurements

R_2 and R_2^* were measured in aqueous medium, because the process of embedding MNPs in agarose or other gels can cause aggregation which in turn would distort the size dependence of the MR relaxation rates. Precise measurements of R_2 and R_2^* with MRI takes at least several minutes. During this time span the magnetic dipole-dipole interaction between the aligned magnetic moments of the MNPs can cause chain formation and aggregation as well [20]. Therefore, all samples were individually measured in an NMR spectrometer (Magritek Spinsolve 1 Tesla), allowing R_2 and R_2^* determination within seconds after inserting the sample into the magnetic field. In order to check whether the relaxation rates changed on this time scale, the measurements were repeated several times within one minute after inserting the samples.

To obtain the relaxation curves, an FID (90° pulse) was acquired for R_2^* while for R_2 a CPMG sequence was used (echo time 200 μ s, 10000–20000 echoes). The relaxation rates were extracted by fitting $A \times \exp(-tR_2^{(*)}) + B$ to the measured signal decay, with A , B and $R_2^{(*)}$ as free parameters. The curve fitting was performed using Matlab (The MathWorks Inc., Natick, MA, USA). Relaxation rates were finally corrected by the relaxation rates of the solvent and divided by the iron content to get the relaxivities $r_2^{(*)}$.

2.6. Iron analysis

Iron quantification was conducted by means of an UV detector (PN3211, Postnova Analytics GmbH, Germany; $\lambda=280$ nm). To directly quantify the iron content using the UV signal, calibration runs with MNPs of different sizes were performed.

2.7. Measurement uncertainties

The x-axis uncertainties shown in all figures represent the uncertainty of the hydrodynamic size determination retrieved from 6 subsequent measurements of the same sample. The uncertainty of the MPS signal results from the standard deviation of the MPS signal obtained from 100 empty sample holder measurements. The uncertainties of the relaxivities have been calculated by uncertainty propagation and are mainly a result of the uncertainty of the iron quantification. The uncertainties of the relaxation curve fitting are included, but negligible. There was no sign of systematic errors.

3. Results and discussion

3.1. Size distributions

Hydrodynamic (d_{Hyd}) and core diameter (d_C) both linearly increased with fraction number for both particle systems.

The hydrodynamic sizes of the fractions combined with the iron quantification yield the size distributions as shown in Fig. 1. The polydispersity index of all fractions was around 0.1. The distribution of the Endorem® fractions was fitted with a log-normal function. If the assumption of a log-normal distribution is correct, the smallest fractions with the highest iron content were not collected after A4F.

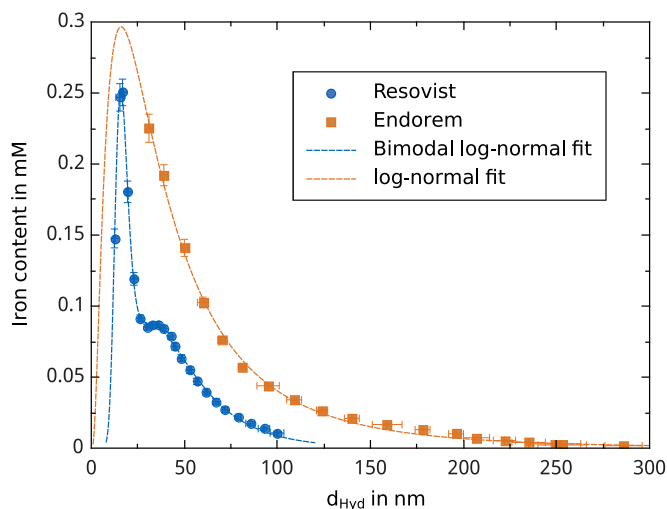


Fig. 1. Hydrodynamic size distribution (z-average) determined by DLS analysis of the fractions.

For Resovist®, the presence of a bimodal distribution of size was confirmed [21]. In general, the Endorem® particles are bigger than the Resovist® particles.

The distributions of the core sizes of the fractions are shown in Fig. 2. Note that the lower size limit of MALS is around $d_c \approx 20$ nm. Both distributions were fitted with a log-normal function.

For the Resovist® fractions, d_C was smaller than d_{Hyd} , enabling us to derive a shell thickness of about 6.5 nm. For the Endorem® fractions, the two size parameters were the same within the measurement uncertainty which indicates that the shell thickness is negligible compared to the overall particle size.

3.2. Magnetic particle spectroscopy

Fig. 3 shows the spectral moment μ_3 of the fractions as determined by MPS. There is a strong nonlinear MPS signal dependence on the MNP size indicating different magnetic structures of the fractions. This is in accordance with other studies [13,17]. There is a maximal spectral moment for Resovist®, while μ_3 of Endorem® saturates with increasing particle size. In addition, the spectral moment of Endorem® is much smaller than that of Resovist®. Since the size parameters of Endorem® are relatively big, the smaller spectral moment can be a result of the dipole-dipole interaction between the single cores within the multi-core structure. This interaction could also explain the drop of the spectral

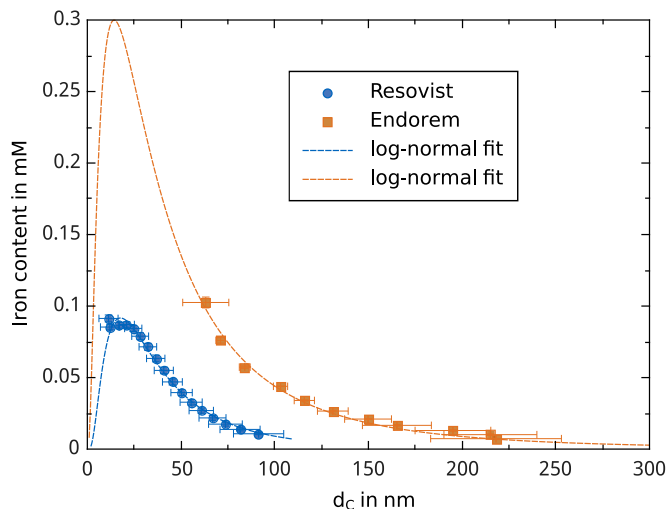


Fig. 2. Core size distribution determined by MALS analysis of the fractions.

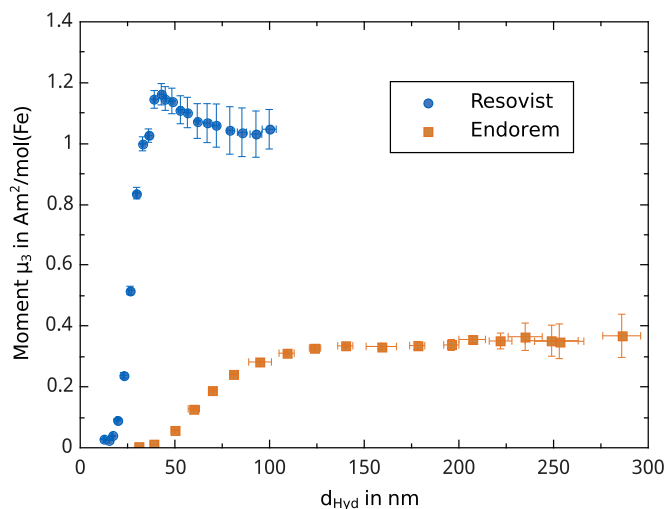


Fig. 3. Spectral moment μ_3 of the fractions as determined by magnetic particle spectroscopy and normalized by the iron content. d_{Hyd} represents the z-average.

moment of Resovist® at bigger diameters.

The MPS spectral moment cannot directly be related to the particle magnetization M_S relevant for MR relaxation because MPS measures the magnetic response of the MNPs to a sinusoidal excitation field at a frequency of 25 kHz. Models to describe the MPS signal behaviour of MNPs and extract magnetic parameters like M_S are a subject of ongoing research [22,23].

3.3. Relaxivities

The results of the relaxation rate measurements for Resovist® are shown in Fig. 4. Since the iron content of the size fractions differs, the relaxivities are shown here to be able to compare the relaxation effect of the fractions. The theoretical predictions for the relaxation rates can be rewritten for the relaxivities as well [8]. Both relaxivities exhibit a strong dependence on the hydrodynamic size. For smaller MNPs, r_2 and r_2^* are very similar and increase with increasing particle size. This is in accordance with the motional averaging regime or outer sphere theory (Eq. (1)). For larger MNPs, r_2 is considerably smaller than r_2^* and seems to reach saturation. This could be explained by the very short refocusing pulses (echo time 200 μs) already becoming effective and might indicate an early onset of the partial refocusing regime (Eq. (3)). The r_2^* trend for these MNPs is not so obvious because of the stronger scattering of the measured values. However, it can be safely

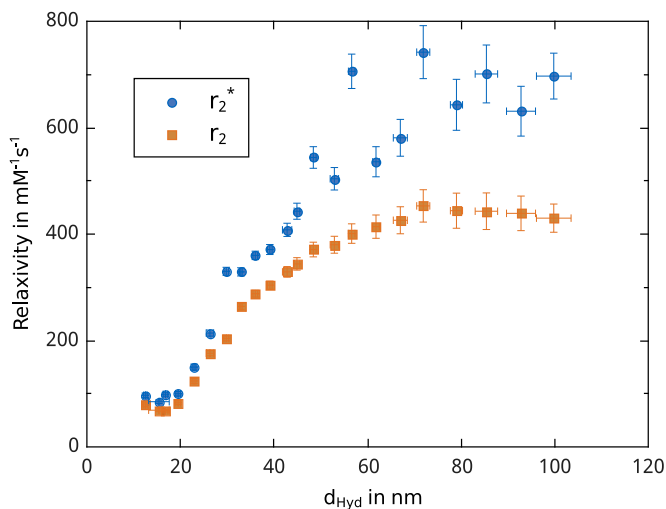


Fig. 4. MR relaxivities of the size fractionated Resovist® particles.

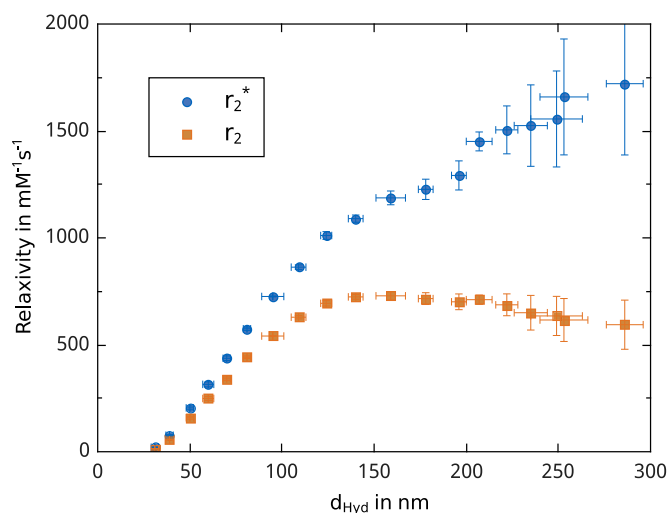


Fig. 5. MR relaxivities of the size fractionated Endorem® particles.

stated that MNPs up to a diameter of 70 nm do not fulfill the condition of static dephasing because of the drastic increase of r_2^* relaxivities. With respect to iron content, these particles represent 88% of the unfractionated sample, which was calculated by integrating the bimodal log-normal function shown in Fig. 1.

The results for Endorem® are shown in Fig. 5 and are essentially identical to those of Resovist®. For smaller MNPs, r_2 and r_2^* are similar and for larger particles r_2 saturates. Despite the larger sizes of the Endorem® fractions compared to Resovist®, no saturation of r_2^* is observable within the measurement uncertainty. Particles up to a diameter of at least 150 nm fall into the motional averaging regime and thus do not meet the static dephasing condition. These particles represent 93% of the unfractionated sample. r_2 seems to slightly decrease for the largest fractions which would be a strong indicator for the partial refocusing regime. However, this drop is close to the significance threshold.

As mentioned in Section 2.5, the relaxation rate measurements were repeated several times after inserting the samples into the magnet. The change of relaxation rates within one minute turned out to be less than 3% for R_2^* and less than 5% for R_2 . The values shown in Figs. 4 and 5 were obtained within 10 s after inserting the samples and can therefore be considered reliable.

Due to the complex multi-core structure of the MNPs investigated here the measured relaxivities could only be qualitatively explained by the analytical equations given in the introduction. Complications may arise from the assumptions of the formulas presupposing uncoated spherical MNPs without size distribution. These assumptions are not applicable here. If the shell thickness is constant for all MNP sizes as observed for Resovist®, the overall magnetization M_S of a particle increases with increasing size. In return, a decreasing packing density of a multi-core particle reduces its content of magnetizable material. The overall magnetization of a particle determines its stray field and thus the influence on the surrounding water protons, which in turn is responsible for MR relaxation. The MPS results indicate different magnetic structures of Resovist® and Endorem® fractions even at the same hydrodynamic size.

4. Conclusion

The combination of hydrodynamic fractionation, geometric and magnetic characterization and MR relaxometry is ideally suited to characterize complex MNP systems with regard to quantitative MRI. The experiments presented here qualitatively confirm the outer sphere relaxation theory for small MNPs. We have shown that the majority of Resovist® and Endorem® particles do not meet the condition for static

dephasing which is a precondition for reliable quantification based on MRI relaxometry. Thus, neither Resovist® nor Endorem® provide MNP systems capable of reliable quantitative MRI, since potential size alteration strongly affects MNP relaxivity.

We expect our approach to facilitate the choice of MNPs for quantitative MRI and to help clarifying the relationship between size, magnetism and relaxivity of MNPs in the future. MPS combined with methods for particle size analysis has the potential to reveal important particle properties of MNPs (e.g. M_S) provided that adequate models for the signal behaviour are available. MPS also allows for a direct control of the MPI performance of a particle system or its size fractions. Additional characterization methods enabling the determination of morphology and packing density of multi-core MNPs, e.g. transmission electron microscopy or X-ray diffraction, are essential for a deeper understanding of the relaxation behaviour and could allow for a quantitative comparison of MR relaxation theories with relaxation measurements.

Acknowledgments

The authors like to thank Stephan Düwel and Christian Hundshammer for their help with the relaxation measurements. Financial support by the EU FP7 Project NanoMag (Grant no. 604448) is gratefully acknowledged.

References

- [1] Q.A. Pankhurst, N.T.K. Thanh, S.K. Jones, J. Dobson, Progress in applications of magnetic nanoparticles in biomedicine, *J. Phys. D: Appl. Phys.* 42 (2009) 224001. <http://dx.doi.org/10.1088/0022-3727/42/22/224001>.
- [2] B. Gleich, T. Weyh, B. Wolf, Magnetic drug targeting: an analytical model for the influence of blood properties on particle trajectories, *Appl. Rheol.* 18 (2008) 52023.
- [3] S. Laurent, S. Boutry, I. Mahieu, L. Vander Elst, R.N. Muller, Iron oxide based MR contrast agents: from chemistry to cell labeling, *Curr. Med. Chem.* 16 (35) (2009) 4712–4727. <http://dx.doi.org/10.2174/092986709789878256>.
- [4] P. Gillis, F. Moyno, R.A. Brooks, On T2-shortening by strongly magnetized spheres: a partial refocusing model, *Magn. Reson. Med.* 47 (2002) 257–263.
- [5] R.N. Muller, P. Gillis, F. Moyno, A. Roch, Transverse relaxivity of particulate MRI contrast media: from theories to experiments, *Magn. Reson. Med.* 22 (1991) 178–182.
- [6] Q.L. Vuong, P. Gillis, Y. Gossuin, Monte carlo simulation and theory of proton nmr transverse relaxation induced by aggregation of magnetic particles used as MRI contrast agents, *J. Magn. Reson.* 212 (2011) 139–148.
- [7] A. Roch, Y. Gossuin, R.N. Muller, P. Gillis, Superparamagnetic colloid suspensions: water magnetic relaxation and clustering, *J. Magn. Magn. Mater.* 293 (2005) 532–539.
- [8] Q.L. Vuong, J.-F. Berret, J. Fresnais, Y. Gossuin, O. Sandre, A universal scaling law to predict the efficiency of magnetic nanoparticles as MRI T2-contrast agents, *Adv. Healthc. Mater.* 1 (2012) 502–512.
- [9] J.B. Haun, T.-J. Yoon, H. Lee, R. Weissleder, Magnetic nanoparticle biosensors, *WIREs Nanomed. Nanotechnol.* 2 (2010) 291–304.
- [10] D.A. Yablonskiy, E.M. Haacke, Theory of NMR signal behavior in magnetically inhomogeneous tissues: the static dephasing regime, *Magn. Reson. Med.* 32 (1994) 749–763.
- [11] C.V. Bowen, X. Zhang, G. Saab, P.J. Gareau, B.K. Rutt, Application of the static dephasing regime theory to superparamagnetic iron-oxide loaded cells, *Magn. Reson. Med.* 48 (2002) 52–61.
- [12] D. Eberbeck, F. Wiekhorst, S. Wagner, L. Trahms, How the size distribution of magnetic nanoparticles determines their magnetic particle imaging performance, *Appl. Phys. Lett.* 98 (18) (2011) 182502. <http://dx.doi.org/10.1063/1.3586776>.
- [13] N. Löwa, P. Radon, D. Gutkelch, R. August, F. Wiekhorst, Hyphenation of field-flow fractionation and magnetic particle spectroscopy, *Chromatography 2* (4) (2015) 655–668. <http://dx.doi.org/10.3390/chromatography2040655>.
- [14] C.W. Jung, P. Jacobs, Physical and chemical properties of superparamagnetic iron oxide MR contrast agents: ferumoxides, ferumoxtran, ferumoxsil, *Magn. Reson. Imaging* 13 (5) (1995) 661–674. [http://dx.doi.org/10.1016/0730-725X\(95\)00024-B](http://dx.doi.org/10.1016/0730-725X(95)00024-B).
- [15] M.F. Casula, P. Floris, C. Innocenti, A. Lascialfari, M. Marinone, M. Corti, R.A. Sperling, W.J. Parak, C. Sangregorio, Magnetic resonance imaging contrast agents based on iron oxide superparamagnetic ferrofluids, *Chem. Mater.* 22 (5) (2010) 1739–1748. <http://dx.doi.org/10.1021/cm9031557>.
- [16] J. Lohrke, Herstellung und Charakterisierung neuer nanopartikularer SPIO-Kontrastmittel fuer die Magnetresonanztomographie (Ph.D. Thesis), Martin-Luther-Universität: Halle-Wittenberg, 2010.
- [17] R.M. Ferguson, A.P. Khandhar, K.M. Krishnan, Tracer design for magnetic particle imaging (invited), *J. Appl. Phys.* 111 (7) (2012) 07B318. <http://dx.doi.org/10.1063/1.3676053>.

- [18] P.J. Wyatt, Mean square radius of molecules and secondary instrumental broadening, *J. Chromatogr. A* 648 (1) (1993) 27–32. [http://dx.doi.org/10.1016/0021-9673\(93\)83285-Z](http://dx.doi.org/10.1016/0021-9673(93)83285-Z).
- [19] N. Löwa, F. Wiekhorst, I. Gemeinhardt, M. Ebert, J. Schnorr, S. Wagner, M. Taupitz, L. Trahms, Cellular uptake of magnetic nanoparticles quantified by magnetic particle spectroscopy, *IEEE Trans. Magn.* 49 (1) (2013) 275–278. <http://dx.doi.org/10.1109/TMAG.2012.2218223>.
- [20] D.-X. Chen, G. Via, F.-J. Xu, C. Navau, A. Sanchez, Waiting time dependence of T2 of protons in water suspensions of iron-oxide nanoparticles: measurements and simulations, *J. Appl. Phys.* 110 (2011) 73917.
- [21] A.F. Thünemann, S. Rolf, P. Knappe, S. Weidner, In situ analysis of a bimodal size distribution of superparamagnetic nanoparticles, *Anal. Chem.* 81 (1) (2009) 296–301. <http://dx.doi.org/10.1021/ac802009q>.
- [22] F. Ludwig, H. Remmer, C. Kuhlmann, T. Wawrzik, H. Arami, R.M. Ferguson, K.M. Krishnan, Self-consistent magnetic properties of magnetite tracers optimized for magnetic particle imaging measured by ac susceptometry, magnetorelaxometry and magnetic particle spectroscopy, *J. Magn. Magn. Mater.* 360 (2014) 169–173. <http://dx.doi.org/10.1016/j.jmmm.2014.02.020>.
- [23] M. Graeser, K. Bente, T.M. Buzug, Dynamic single-domain particle model for magnetite particles with combined crystalline and shape anisotropy, *J. Phys. D: Appl. Phys.* 48 (27) (2015) 275001. <http://dx.doi.org/10.1088/0022-3727/48/27/275001>.